JACS
JOURNAL OF THE AMERICAN CHEMICAL SOCIETY
pubs.acs.org/JACS
Article

Signatures of the Bromine Atom and Open-Shell Spin Coupling in the X-ray Spectrum of the Bromobenzene Cation

Michael Epshtein, Bruno Nunes Cabral Tenorio, Marta L. Vidal, Valeriu Scutelnic, Zheyue Yang, Tian Xue, Anna I. Krylov, Sonia Coriani, and Stephen R. Leone*

Cite This: J. Am. Chem. Soc. 2023, 145, 3554–3560
Read Online
ACCESS | Metrics & More | Article Recommendations | Supporting Information

ABSTRACT: Tabletop X-ray spectroscopy measurements at the carbon *K*-edge complemented by *ab initio* calculations are used to investigate the influence of the bromine atom on the carbon core–valence transitions in the bromobenzene cation ($BrBz^+$). The electronic ground state of the cation is prepared by resonance-enhanced two-photon ionization of neutral bromobenzene (BrBz) and probed by X-rays produced by high-harmonic generation (HHG). Replacing one of the hydrogen atoms in benzene with a bromine atom shifts the transition from the $1s_{C^*}$ orbital of the carbon atom (C*) bonded to bromine by ∼1 eV to higher energy in the X-ray spectrum compared to the other carbon atoms (C). Moreover, in $BrBz^+$, the X-ray spectrum is dominated by two relatively intense transitions, $1s_C \rightarrow \pi^*$ and $1s_{C^*} \rightarrow \sigma^*(C^*-Br)$, where the second transition is enhanced relative to the neutral BrBz. In addition, a doublet peak shape for these two transitions is observed in the experiment. The $1s_C \rightarrow \pi^*$ doublet peak shape arises due to the spin coupling of the unpaired electron in the partially vacant π orbital (from ionization) with the two other unpaired electrons resulting from the transition from the $1s_C$ core orbital to the fully vacant π^* orbitals. The $1s_{C^*} \rightarrow \sigma^*$ doublet peak shape results from several transitions involving σ^* and vibrational C*–Br mode activations following the UV ionization, which demonstrates the impact of the C*–Br bond length on the core–valence transition as well as on the relaxation geometry of $BrBz^+$.

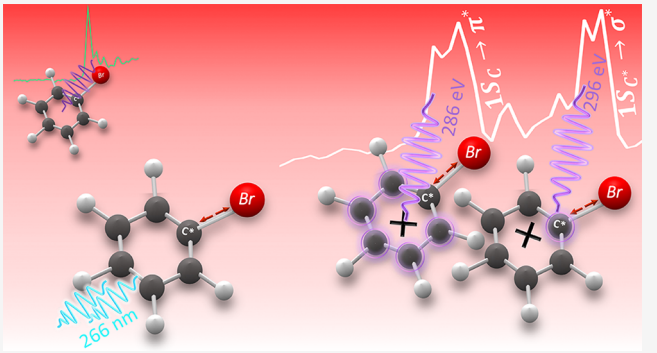

INTRODUCTION

X-ray spectroscopy at the carbon K-edge is highly sensitive to the changes in molecular structure and orbital occupancy, delivering accurate information about the energy of core and valence orbitals of molecules containing carbon atoms. The ability to laser-produce tabletop HHG sources reaching up to 300 eV opened opportunities to implement the laser pump-probe technique with ultraviolet (UV) excitation probed by soft X-ray radiation in the carbon *K*-edge region with tens of femtosecond time resolution.[1−8]

Recently, we applied this technique to measure the X-ray spectrum of the benzene radical cation (Bz^+).[9] Together with high-level calculations using equation-of-motion coupled-cluster singles and doubles theory (EOM-CCSD), this study provided insight into the electronic structure of benzene (Bz) and its cation.[10] Comparison of the X-ray absorption spectra of neutral Bz and of Bz^+ revealed a splitting of the two degenerate π^* orbitals as well as an appearance of a new peak due to a new transition to the partially occupied π orbital resulting from the ionization. According to the calculations, the observed splitting in the cation spectrum was ascribed primarily to the spin coupling of the unpaired electron in the partially vacant π orbital with the unpaired electrons resulting from the excitation of one of the carbon 1s electrons to the vacant π^* orbitals.[9,10] Jahn–Teller (JT) relaxation causing symmetry distortion was also considered.

Replacing one of the hydrogen atoms of Bz with a bromine atom lowers the D_{6h} point-group symmetry of neutral Bz to C_{2v} and also lifts the near-degeneracies between the six core orbitals of the carbon atoms. In particular, the Br atom increases the transition energy of the carbon atom bonded to the bromine atom, here labeled as C*. The two highest occupied molecular orbitals, $\pi(6b_2)$ and $\pi(2a_2)$, result from a splitting of the highest degenerate π orbitals of Bz. The highest occupied molecular orbital (HOMO) $\pi(6b_2)$, with the lowest binding energy of 8.992 eV,[11] shows partial bromine character.[12−14] The major electron density of the $\pi(6b_2)$ orbital is distributed among several atoms, the C* atom (0.46), the C atom that is in the para position to C* (0.5), the Br

Received: November 21, 2022
Published: February 3, 2023

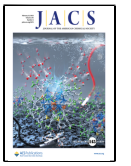

https://doi.org/10.1021/jacs.2c12334
J. Am. Chem. Soc. 2023, 145, 3554−3560

atom (0.47), and among the other C atoms (0.56).[12] The next lower $\pi(2a_2)$ orbital of BrBz is noticeably shifted to lower energy (i.e., to higher binding energy, 9.663 eV) compared to the parent π orbital of Bz. The next two lower molecular orbitals are $11b_1$ (σ_{Br}-type) and $5b_2$ (π_{Br}-type), which are related to the 4p bromine lone pair orbitals, which are split due to the interaction with the benzene ring.[12−14] The ionization energies from these two orbitals are 10.633 and 11.188 eV, respectively.[13]

The bromine atom affects the core-level transition energies as well. Previous studies have shown that[15] the 1s orbital of the carbon atom (C*) nearest to the bromine atom is shifted to higher binding energy by about 1.1 eV relative to the 1s orbitals of the other carbons (C), as shown in the orbital diagram of BrBz in Figure 1. The splitting of the other $1s_C$ orbitals due to the lower symmetry of the benzene ring is much smaller.[15] The different electron distribution in the valence and core levels due to bromine attachment leads to several changes in the X-ray spectrum of neutral BrBz compared to Bz.[15] The major change appears as a new peak related to the $1s_{C^*}\rightarrow\pi^*$ transition shifted to higher energy by about 1.1 eV from the most intense peak that corresponds to the $1s_C\rightarrow\pi^*$ transition, which is similar to the $1s_C\rightarrow\pi^*$ transition in the X-ray spectrum of neutral Bz.

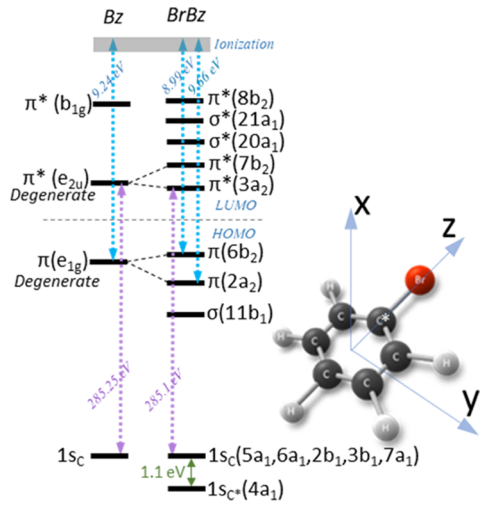

Figure 1. Schematic orbital diagram of neutral Bz and BrBz based on refs 11, 15 with relevant ionization energies and core−valence transition energies (the energy is not to scale). The geometry of BrBz and the coordinate system are shown on the right. The molecule is in the *YZ* plane with Br on the *Z* axis. The carbon atom binding to Br is labeled as C*.

The effect of substitution of the bromine atom (as well as other halogen atoms) in neutral aromatic rings on the core−valence transitions in the carbon *K*-edge region has been investigated in the past.[15−18] In contrast, the influence of halogen atoms on the core−valence transitions at the carbon *K*-edge in the cations has not been studied before. In this work, we examine the influence of a bromine atom on the core−valence transitions in $BrBz^+$ by comparing the experimental near-edge X-ray absorption fine structure spectrum (NEXAFS) of $BrBz^+$ with the spectrum of neutral BrBz and with our recent spectrum of Bz^+ in the same energy region,[9,10] combined with electronic structure calculations. Specifically, we used the density functional theory/restricted open-shell configuration interaction singles (DFT/ROCIS) method,[19] associated with molecular dynamics (MD) simulations using the B3LYP functional,[20] and the def2-TZVP basis set.[21] Ground and excited states of $BrBz/BrBz^+$ are calculated as pure singlet/doublet states at the DFT/ROCIS level.[19] As typically done, all computed core spectra were shifted (by 10.2 eV for the neutral and 9.2 eV for the cation) to align them with their experimental counterparts. These global shifts correct for the systematic errors due to the incomplete description of relaxation effects after the creation of the core hole and relativistic effects in the DFT/ROCIS approach.

RESULTS

The experimental spectrum of neutral BrBz, presented in Figure 2a, is obtained from $A = \log(I_{\text{without Bz}}/I_{\text{with Bz}})$, where $I_{\text{without Bz}}$ and $I_{\text{with Bz}}$ are the transmitted signal of the broadband X-ray flux without BrBz molecules in the interaction region and with a flow of BrBz molecules at room temperature, respectively, as described in detail previously.[3,9] The spectrum matches well with previously reported results,[15] and it agrees with our calculations, shown in red in Figure 2b (ROCIS) and in Figure S7 (EOM-CCSD) in the Supporting Information (SI). The spectrum exhibits one dominant peak at 285.1 eV, labeled as A in Figure 2a, followed by at least four discernable peaks of lower intensity, labeled B−E.

In accordance with the previous work, we assign peak A to transitions from the $1s_C$ orbitals (i.e., the 1s orbitals of the C atoms not bound to the Br atom) to the two lowest unoccupied π^* molecular orbitals,[15] similar to the $1s_C\rightarrow\pi^*$ transition observed at 285.25 eV in the X-ray spectrum of Bz[9,10,13,15] (see Table 1 for details on the peak assignments and calculated energies).

We ascribe the next, less intense, observed transition peak B at 286.2 eV to an electronic transition from the $1s_{C^*}$ orbital ($4a_1$) to π^*. Hitchcock et al.[15] also assigned this peak to a $1s_{C^*}\rightarrow\pi^*$ transition and concluded that the energy shift between peaks A and B occurs primarily due to the chemical shift (of about 1.1 eV stronger binding) of the $1s_{C^*}$ orbital relative to the $1s_C$ orbitals, while the energy of the π^* orbital is insensitive to bromine substitution. Similar behavior was observed in chlorobenzene (ClBz),[22] iodobenzene (IBz), and fluorobenzene (FBz).[15]

The influence of the halogen substitution on the 1s orbital of the nearest carbon atom (C*) has been explored in several other studies.[16−18] For instance, by replacing the number of F atoms with hydrogens, Hitchcock et al.[16] and Plashkevych et al.[18] showed that the relative intensities of $1s_C\rightarrow\pi^*$ and $1s_{C^*}\rightarrow\pi^*$ transitions are affected by the relative number of C and C* carbon sites. Interestingly, the position of the $1s_C\rightarrow\pi^*$ and $1s_{C^*}\rightarrow\pi^*$ transitions was almost unaffected by the change in the number of F atoms, indicating the localized behavior of the $1s_C$ and $1s_{C^*}$ orbitals and the insensetivity of the energy of the π^* orbital to the substitution. In addition, it was proposed by Hitchcock et al. and by Schwarz et al. that a $1s_C\rightarrow3s$ transition contributes to the intensity of the peak assigned to the $1s_{C^*}\rightarrow\pi^*$ transition.[16,17] Similarly, $1s_C\rightarrow\pi^*$ and $1s_{C^*}\rightarrow\pi^*$ transitions are reported in the X-ray spectrum of C_3H_2Br to have similar amplitude ratio, emphasizing the dependence of the peak intensities on the number of core sites and the localized behavior near the C*−Br bond.[23] Our computed $1s_{C^*}\rightarrow\pi^*$ transition energy matches well the experimental result, aside from a slightly larger separation between peaks A and B, as can be seen from Figure 2a,b. Next, peak C in Figure 2a is observed

https://doi.org/10.1021/jacs.2c12334
J. Am. Chem. Soc. 2023, 145, 3554−3560

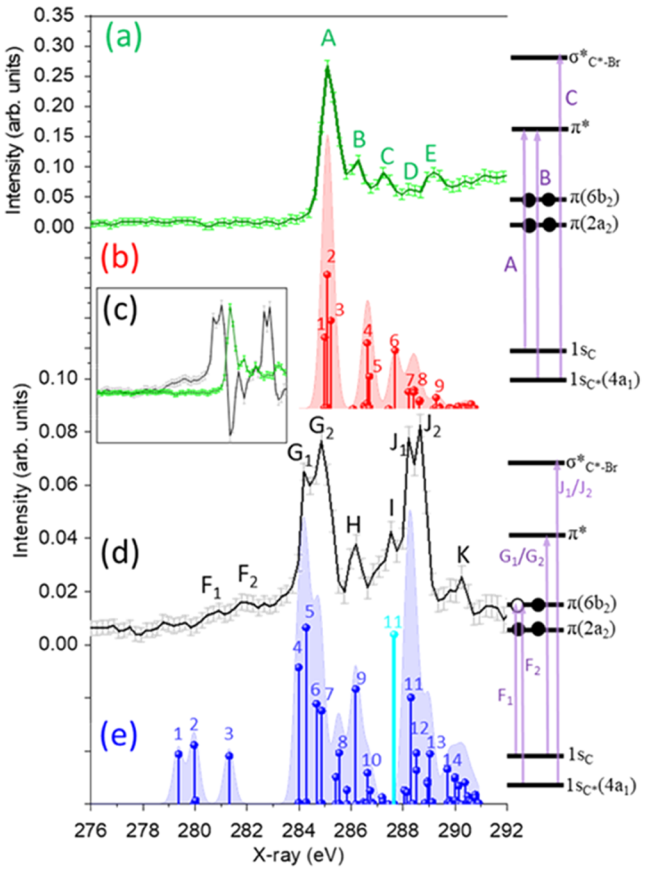

Figure 2. (a) Experimental NEXAFS spectrum of ground-state neutral BrBz (green line with light green error bars corresponding to 95% confidence interval limits). The spectrum is an average of 256 CCD images (1000 laser pulses per image). The full range of the same data is presented in the Supporting Information (SI). (b) Calculated DFT-ROCIS transitions of neutral BrBz shown by red sticks and the corresponding broadened spectrum (shifted by +10.2 and 0.45 eV Gaussian width for each transition). (c) Experimental NEXAFS spectra of neutral BrBz (green) and of $BrBz^+$ (black). The spectrum is an average of 768 CCD images (see SI for details). (d) NEXAFS spectrum of $BrBz^+$ obtained by adding 20% of the static neutral BrBz spectra (see SI for details) to the difference spectrum ΔA in (c), taken at ∼1 ps delay, represented by the black line with gray error bars, and with the energy diagram on the right side. (e) Calculated DFT-ROCIS transitions of $BrBz^+$ at relaxed geometry (blue sticks) and the corresponding broadened spectrum (shifted by 9.2 and 0.45 eV Gaussian width for each transition). The calculations were performed with B3LYP/def2-TZVP without making use of the symmetry point group. The cyan stick in (e) corresponds to the $1s_{C^*} \rightarrow \sigma^*(C^*-Br)$ transition at the equilibrium geometry (EG) of the ground state of the neutral species. The full spectrum at this geometry is shown in Figure S2 in SI. The energy diagram on the side illustrates the major transitions observed in the spectra.

at around 287 eV. The calculations suggest that this peak is related to the $1s_{C^*} \rightarrow \sigma^*(C^*-Br)$ transition labeled as 6 in Figure 2b. The other transitions correspond to peaks D and E, and to sticks 7−9, as shown in Table 1, with some similarity to the previous calculation for Bz.[24] The binding energies were reported in previous works to be 290.5 and 291.3 eV from $1s_C$ and $1s_{C^*}$, respectively.[15,25]

The black line in Figure 2d shows the absorption spectrum of $BrBz^+$. The spectrum is obtained from $\Delta A = \log(I_{\text{without UV}}/I_{\text{with UV}})$, where $I_{\text{without UV}}$ and $I_{\text{with UV}}$ are the transmitted signal of the X-ray flux without UV and with UV, respectively, after

Table 1. Transitions of Neutral BrBz Observed in the Experimental Spectrum in Figure 2a Compared with the Computed Transitions Shown as Sticks in Figure 2b[a]

Experiment		ROCIS-DFT		
Peak	Energy (eV)	Stick	Energy (eV)	Assignment
A	285.1	1	285.03	$1s_C(3b_1) \rightarrow \pi^*(3a_2)$; $1s_C(6a_1) \rightarrow \pi^*(7b_2)$
		2	285.22	$1s_C(2b_1) \rightarrow \pi^*(3a_2)$; $1s_C(5a_1) \rightarrow \pi^*(7b_2)$
		3	285.24	$1s_C(7a_1) \rightarrow \pi^*(7b_2)$
B	286.2	4	286.56	$1s_{C^*}(4a_1) \rightarrow \pi^*(7b_2)$
		5	286.64	$1s_C(3b_1) \rightarrow \sigma^*(20a_1)$
C	287.1	6	287.57	$1s_{C^*}(4a_1) \rightarrow \sigma^*(20a_1)$
D	288.0	7	288.05	$1s_C(7a_1) \rightarrow \sigma^*(21a_1)$
		8	288.24	$1s_C(3b_1) \rightarrow \sigma^*(20a_1)$; $1s_C(3b_1) \rightarrow \sigma^*(21a_1)$
E	288.5	9	289.04	$1s_C(2b_1) \rightarrow \sigma^*(21a_1)$

[a]Calculated energies shifted by 10.2 eV to align with the experimental spectrum.

adding back 20% of the neutral spectrum. The UV pulses at 267 nm ionize the molecule by resonance-enhanced two-photon ionization (1+1 REMPI) after being focused with a 45 cm f.l. lens where the UV pulse energy is ∼25 μJ. The broadband HHG pulse near the carbon K-edge probes the prepared $BrBz^+$ after a ∼1 ps time delay. Two-photon 267 nm excitation is in resonance with several low vibrational states of the first ionized state,[11,26] in which one electron is removed from the π orbital, creating a hole in the highest $\pi(6b_2)$ orbital. Consequently, the lowest-energy transition (at ∼281 eV) in the cation from a core orbital is of $1s_C \rightarrow \pi$ character, while a second transition (of $1s_{C^*} \rightarrow \pi$ character) is expected to be ∼1 eV higher in energy. Evidence of these two transitions is barely discernible in the experimental spectrum. The core-to-SOMO (singly occupied MO) $1s_C \rightarrow \pi$ transition in Bz^+ was found to be relatively weak in our previous study,[9] and it is expected to be even weaker in $BrBz^+$ because the intensity is redistributed between two transitions from $1s_C$ and $1s_{C^*}$ orbitals, in addition to possibly a more diffuse vibrational structure due to higher available energy (E_{av}) after ionization ($E_{ph} - E_{Ion} = E_{av} = 0.25$ eV compared to 0.07 eV in Bz^+). Indeed, theory shows the

https://doi.org/10.1021/jacs.2c12334
J. Am. Chem. Soc. 2023, 145, 3554−3560

presence of two major transitions from $1s_C$, namely, $1s_C(7a_1)\rightarrow\pi(6b_2)$, $1s_C(5a_1)\rightarrow\pi(6b_2)$, in addition to the $1s_{C^*}(4a_1)\rightarrow\pi(6b_2)$ transition at higher energy (blue sticks labeled 1−3 in Figure 2e and Table 2). However, due to the weak intensity of several relevant transitions and diffuse vibrational structure that was not considered in the calculation, there is an offset between the measured and calculated transitions.

The next two peaks of nearly equal intensity, toward higher energy, a doublet peak structure, are labeled as G_1 and G_2 at 283.9 and 284.55 eV (0.65 eV difference), respectively, and are readily seen in the raw data inset in Figure 2c for $BrBz^+$ even before adding back 20% of the neutral BrBz spectrum. These peaks are red-shifted compared to peak A ($1s_C\rightarrow\pi^*$) of BrBz, and it is therefore reasonable to assign them to $1s_C\rightarrow\pi^*$ transitions, similar to the previously reported Bz^+ spectrum.[9] Indeed, the transitions from $1s_C$ to the lowest π^* orbital observed in the X-ray spectrum of neutral Bz and of BrBz are remarkably similar and the energy of the π^* orbital is not affected by replacing halogen atoms as pointed out above; the same is expected to occur in the X-ray spectrum of the cations. The doublet peak structure of G_1 and G_2 can be (partly) explained by the spin coupling of the three unpaired electrons,[27,28] as recently observed in N_2^+,[29] CO^+,[30] and Bz^+.[9,10] The splitting of the main peak in Bz^+ is more than 1 eV, caused mostly by spin coupling between unpaired electrons in $1s_C$, π, and π^* orbitals as substantiated by the calculations.[10] The theoretical results have shown that Jahn−Teller (JT) shifts for Bz^+ cause a much smaller splitting of the two degenerate π^* orbitals. Here, we attribute the observed doublet peak structure of $BrBz^+$ to a similar spin-coupling effect. The calculations revealed the presence of two transitions from two different $1s_C$ orbitals to π^* (sticks 4 and 5 in Figure 2e and the corresponding assignments in Table 2), followed by a transition $1s_C(7a_1)\rightarrow\pi^*(3a_2)$ (stick 6) plus two transitions, labeled as sticks 7 and 8, involving the same orbitals as sticks 4 and 5 but with different spins of the unpaired electrons in the π orbital (SOMO).

The next peak, labeled as H, fits well to the calculated $1s_C\rightarrow\sigma^*(C^*-Br)$ transition (labeled as stick 9), with an additional contribution from a $1s_{C^*}\rightarrow\pi^*$ transition (stick 10). This behavior is quite similar to the neutral BrBz, while in $BrBz^+$, the calculations show a more dominant influence of the transition to the $\sigma^*(C^*-Br)$ orbital. The next dominant transitions in the experimental spectrum are labeled as peaks J_1 and J_2 at 288.2 and 288.60 eV, respectively. In the previously reported X-ray spectrum of Bz^+,[9] we did not observe major peaks in this energy region and therefore consider these transitions as strongly related to the bromine atom.

The effect of the bromine atom on the transitions related to the benzene ring is small, as can be seen by comparing the $1s_C\rightarrow\pi^*$ transition in the neutral Bz and BrBz X-ray spectra, which are similar. The same conclusion can be drawn from the fluorinated benzene X-ray spectrum as mentioned previously,[16] as a change in the number of the fluorine atoms had no effect on the energy of the $1s_C\rightarrow\pi^*$ transition. Therefore, the major effect of the bromine atom should be related to the C*−Br bond, in particular, on the transition to the orbitals related to this bond, for example, $1s_{C^*}\rightarrow\sigma^*(C^*-Br)$.

Above 287 eV, the experimental spectrum of the cation is dominated by the split bands J_1 and J_2. According to our calculations, the most intense transition in this region is due to $1s_{C^*}\rightarrow\sigma^*(C^*-Br)$, which in neutral BrBz corresponds to band

Table 2. Transitions of $BrBz^+$ Observed in the Experimental Spectrum in Figure 2d and in the Calculated Sticks in Figure 2e[a]

Experiment		ROCIS-DFT		
Peak	Energy (eV)	Stick	Energy (eV)	Assignment
F	280.70 281.80	1	279.37	$1s_C(7a_1)$ → $\pi(6b_2)$, somo
		2	279.97	$1s_C(5a_1)$ → $\pi(6b_2)$, somo
		3	281.32	$1s_{C^*}(4a_1)$ → $\pi(6b_2)$, somo
G_1	284.20	4	283.99	$1s_C(3b_1)$ → $\pi^*(3a_2)$; $1s_C(6a_1)$ → $\pi^*(7b_2)$
		5	284.27	$1s_C(2b_1)$ → $\pi^*(3a_2)$; $1s_C(5a_1)$ → $\pi^*(7b_2)$
G_2	284.85	6	284.68	$1s_C(7a_1)$ → $\pi^*(7b_2)$
		7	284.87	$1s_C(3b_1)$ → $\pi^*(3a_2)$; $1s_C(6a_1)$ → $\pi^*(7b_2)$
		8	285.49	$1s_C(2b_1)$ → $\pi^*(3a_2)$; $1s_C(5a_1)$ → $\pi^*(7b_2)$
H	286.20	9	286.18	$1s_C(2b_1)$ → $\sigma^*(20a_1)$
		10	286.63	$1s_{C^*}(4a_1)$ → $\pi^*(7b_2)$
EG		11'	287.66	$1s_{C^*}(4a_1)$ → $\sigma^*(20a_1)$
J_1	288.20	11	288.31	$1s_{C^*}(4a_1)$ → $\sigma^*(20a_1)$
J_2	288.60	12	288.52	$1s_C(3b_1)$ → $\sigma^*(21a_1)$
		13	289.04	$1s_C(7a_1)$ → $\sigma^*(20a_1)$
k	290.2	14	289.70	$1s_C(6a_1)$ → $\pi^*(8b_2)$

[a]The calculated transition at the ground-state equilibrium geometry of BrBz (EG in the table) is not observed in the experimental spectrum due to a long-time delay. The highlighted sticks 4, 7 (orange) and 5, 8 (blue) are different in energy due to spin coupling. Calculated energies shifted by 9.2 eV to fit the experimental spectrum.

https://doi.org/10.1021/jacs.2c12334
J. Am. Chem. Soc. 2023, 145, 3554−3560

C. We note that after ionization, a major change in the cation's ground-state structure relative to the neutral ground-state BrBz appears to be the C*−Br bond length, which changes from 1.9189 to 1.8439 Å (according to our calculated geometries obtained at the MP2/cc-pVTZ and EOM-IP-CCSD/cc-pVTZ levels, see the Supporting Information). This could be one of the reasons for the dramatic change in transition intensities for peaks J_1 and J_2 compared to peaks C and D in neutral BrBz.

Moreover, the transition to a σ^*(C*−Br) orbital may be affected by the vibrational motion of the C*−Br bond. Two-photon excitation imparts vibrational excitation to the cation, even though the exact determination of the excited vibrational state is difficult due to the low spectral resolution of the experimental system, the spectral width of the UV pulses, and due to the high density of the vibrational states at 9.24 eV. However, since the two-photon ionization process is sensitive to the vibrational mode(s) of the (intermediate) electronic excited state of neutral BrBz reached by the first photon excitation, $^1A_1 \rightarrow {}^1B_2$ ($\pi\pi^*$), where the density of possible vibrational states is lower (in the region reached by one photon), it is possible to predict which vibrational modes of the cation are activated. The transition from the electronic ground state to the ground vibrational state of $^1B_2$ is 4.586 eV. With the first photon (4.64 ± 0.08 eV), it is thus possible to reach the vibrational ground state and excite the C_6H_5−Br stretching mode (ν_{6a} = 0.03645 eV) of the electronic intermediate state ($^1B_2$). It is likely that excited vibrational states of the cation involve the C_6H_5−Br stretching mode (ν_{6a} at 0.047 eV for $BrBz^+$ in the electronic ground state) alone or in combination with other modes, as shown in One-Photon Mass-Analyzed Threshold Ionization (MATI) spectra.[31] Since the experiment is carried out at room temperature, each vibrational mode includes a rich spectrum of rotational transitions, in addition to some hot bands.[11] The excited C*−Br stretching mode may influence the X-ray spectrum by shifting $1s_{C^*}\rightarrow\sigma^*$(C*−Br) transition energies and their intensities, as we observe in $BrBz^+$ compared to the neutral BrBz. DFT-ROCIS calculations based on molecular dynamics simulations have been used to demonstrate the high sensitivity of the $1s_{C^*}\rightarrow\sigma^*$(C*−Br) transition to the stretching mode of the C*−Br bond. The results of these calculations, shown in Figure S6, also illustrate a high sensitivity of the position of the $1s_{C^*}\rightarrow\sigma^*$(C*−Br) transition to the C*−Br bond length. This is also seen by comparing the calculated X-ray spectrum of $BrBz^+$ at the ground-state equilibrium geometry of neutral BrBz assuming the equilibrium geometry of the ground state of neutral BrBz, with the spectrum at the relaxed geometry of the cation (which has, as previously mentioned, a different C*−Br bond length); in particular, the difference in the position of the cyan stick 11′ in Figure 2e, obtained at ground-state equilibrium geometry of BrBz, and stick 11 (peak J_1), which is the same transition but at relaxed geometry of $BrBz^+$. The enhanced sensitivity in energy is observed mostly for the $1s_{C^*}\rightarrow\sigma^*$(C*−Br) transition, while most of the other transitions remain at the same energy, as Figure S6 shows. Based on these results, one can tentatively rationalize the observed double-peaked structure of band J by the initial vibrational C*−Br stretching mode, since the molecule spends most of the time at two different bond lengths along the stretching mode of the C*−Br bond, in addition to the contribution of the other transitions labeled as sticks 12 and 13. The precise assignment of other peaks, including peaks I and K, is difficult due to low intensities and many different possibilities involving different core orbitals and spin coupling effects.

Preparation of $BrBz^+$ in the electronic ground state by two-photon ionization and exclusion of possible contributions due to both one-photon excitation of neutral BrBz and photo-dissociation processes from the first electronic state, as well as three-photon electronically excited cations, are expected to be small enough compared to the discussed observations of this work, similar to our previous study with benzene.[9] The cross section for the intermediate electronic resonance state [$^1A_1 \rightarrow {}^1B_2$ ($\pi\pi^*$), 4.586 eV][31] of BrBz with one photon (266.8 nm) is 3×10^{-19} (cm^2/molecule),[11] is greater than that in Bz (10^{-20}−10^{-21} cm^2/molecule)[32,33] but still small; therefore, the major process driven by fs pulses around 266 nm is REMPI (1+1).[34] Preparation of excited electronic states of $BrBz^+$ may be possible only by transferring an electron from a lower orbital and requiring three photons, as shown in the schematic orbital diagram of neutral BrBz in Figure 2. Moreover, excitation from the lower orbital with a 267 nm photon is below the first resonance (excitation to first electronic state) and therefore expected to be a significantly less probable process. From this, we conclude that the major probed molecules by the X-ray flux are bromobenzene cations in the ground electronic state.

CONCLUSIONS

This work investigated the carbon *K*-edge spectrum of $BrBz^+$ by recording the following resonance ionization with two UV photons on neutral BrBz. The influence of the bromine atom on the X-ray spectrum of $BrBz^+$ is examined together with the spin coupling of the partially vacant 1s core orbital, the partially occupied π orbital, and the partially occupied π^* orbital. In particular, the partially occupied π orbital leads to relatively weak $1s_C\rightarrow\pi$ and $1s_{C^*}\rightarrow\pi$ transitions, while the $1s_C\rightarrow\pi^*$ transitions are observed as a first dominant peak slightly shifted to lower energy compared to corresponding transitions in the neutral BrBz, similarly to the Bz^+ X-ray spectrum. Our results are supported by theoretical calculations by the DFT/ROCIS method. An additional relatively intense doublet peak is observed at higher energy and is assigned to the $1s_{C^*}\rightarrow\sigma^*$(C*−Br) transition of the cation. This transition demonstrates the significant influence of the bromine atom on the X-ray spectrum of $BrBz^+$ compared to Bz^+ and to neutral BrBz. The calculated spectrum reproduces the experimental features, but the big challenge of accurate calculations in large molecules remains together with a need for a better understanding of the spin coupling effect.

The new peaks, J_1/J_2, clearly demonstrate the influence of the bromine atom on the $1s_{C^*}\rightarrow\sigma^*$(C*−Br) transition in $BrBz^+$ and maybe some contribution from the $1s_C\rightarrow\sigma^*$(C−Br) transition. Thus, the ionization from the $\pi(6b_2)$ orbital, which has bromine character, has an impact on the C*−Br bond length and charge distribution near the C*−Br bond, leading to a higher transition probability for $1s_{C^*}\rightarrow\sigma^*$(C*−Br). Moreover, the experimental and calculated spectra show a strong influence on the core-to-valence transition energy of the C*−Br bond length that is altered from the relaxed geometry of $BrBz^+$ and the C*−Br vibrational stretching mode, which is highly active in $BrBz^+$. On the other hand, the influence of the

https://doi.org/10.1021/jacs.2c12334
J. Am. Chem. Soc. 2023, 145, 3554−3560

bromine atom on the rest of the benzene ring, and in particular on the transition to the π^* orbital, is small.

■ ASSOCIATED CONTENT

Supporting Information

The Supporting Information is available free of charge at https://pubs.acs.org/doi/10.1021/jacs.2c12334.

Experimental spectra of neutral BrBz and $BrBz^+$ with and without add-back correction; transient X-ray absorption spectra of $BrBz^+$; transient X-ray spectra after adding different percentages of the static spectrum; power-dependence study; calculated DFT-ROCIS transitions of $BrBz^+$ at equilibrium geometry of the ground state of the neutral species and at the relaxed geometry of the cation; calculated DFT-ROCIS spectrum of $BrBz^+$ based on MD simulations; calculated versus experimental NEXAFS spectra of neutral BrBz at the carbon K-edge; calculated NEXAFS of neutral BrBz obtained at equation-of-motion coupled-cluster singles and doubles fc-CVS-EOMEE-CCSD/6-311(2+,+)G** (uncontracted on C) level of theory; and table with optimized structures of BrBz and $BrBz^+$ (PDF)

■ AUTHOR INFORMATION

Corresponding Author

Stephen R. Leone − *Department of Chemistry, University of California, Berkeley, California 94720, United States; Chemical Sciences Division, Lawrence Berkeley National Laboratory, Berkeley, California 94720, United States; Department of Physics, University of California, Berkeley, California 94720, United States;* orcid.org/0000-0003-1819-1338; Email: SRL@berkeley.edu

Authors

Michael Epshtein − *Department of Chemistry, University of California, Berkeley, California 94720, United States; Chemical Sciences Division, Lawrence Berkeley National Laboratory, Berkeley, California 94720, United States;* orcid.org/0000-0002-9149-3191

Bruno Nunes Cabral Tenorio − *DTU Chemistry—Department of Chemistry, Technical University of Denmark, DK-2800 Kongens Lyngby, Denmark;* orcid.org/0000-0002-9702-998X

Marta L. Vidal − *DTU Chemistry—Department of Chemistry, Technical University of Denmark, DK-2800 Kongens Lyngby, Denmark;* orcid.org/0000-0003-0653-2078

Valeriu Scutelnic − *Department of Chemistry, University of California, Berkeley, California 94720, United States; Chemical Sciences Division, Lawrence Berkeley National Laboratory, Berkeley, California 94720, United States;* orcid.org/0000-0001-9209-1242

Zheyue Yang − *Department of Chemistry, University of California, Berkeley, California 94720, United States;* orcid.org/0000-0002-3446-0860

Tian Xue − *Department of Chemistry, University of California, Berkeley, California 94720, United States*

Anna I. Krylov − *Department of Chemistry, University of Southern California, Los Angeles, California 90089, United States;* orcid.org/0000-0001-6788-5016

Sonia Coriani − *DTU Chemistry—Department of Chemistry, Technical University of Denmark, DK-2800 Kongens Lyngby, Denmark;* orcid.org/0000-0002-4487-897X

Complete contact information is available at: https://pubs.acs.org/10.1021/jacs.2c12334

Notes

The authors declare the following competing financial interest(s): A.I.K. is the president and a part-owner of Q-Chem, Inc.

■ ACKNOWLEDGMENTS

M.E., V.S., Z.Y., T.X., and S.R.L. gratefully acknowledge the generous support from the U.S. Department of Energy, Office of Science, Office of Basic Energy Sciences (Contract No. DEAC02-05CH11231) through the Gas Phase Chemical Physics Program through the Chemical Sciences Division of Lawrence Berkeley National Laboratory. V.S. acknowledges support from the Swiss National Science Foundation (P2ELP2_184414). B.N.C.T. acknowledges support from the European Union's Horizon 2020 Research and Innovation Programme under the Marie Skłodowska-Curie Individual Fellowship (Grant Agreement No. 101027796). A.I.K. acknowledges financial support by the U.S. National Science Foundation through the CHE-2154482 grant. M.L.V. and S.C. acknowledge financial support from the Independent Research Fund Denmark-Natural Sciences, DFF-RP2 grant no. 7014-00258B.

■ REFERENCES

(1) Bhattacherjee, A.; Leone, S. R. Ultrafast X-Ray Transient Absorption Spectroscopy of Gas-Phase Photochemical Reactions: A New Universal Probe of Photoinduced Molecular Dynamics. *Acc. Chem. Res.* **2018**, *51*, 3203−3211.

(2) Pertot, Y.; Schmidt, C.; Matthews, M.; Chauvet, A.; Huppert, M.; Svoboda, V.; Von Conta, A.; Tehlar, A.; Baykusheva, D.; Wolf, J.-P.; Wörmer, H-J. Time-Resolved X-Ray Absorption Spectroscopy with a Water Window High-Harmonic Source. *Science* **2017**, *355*, 264−267.

(3) Attar, A. R.; Bhattacherjee, A.; Pemmaraju, C. D.; Schnorr, K.; Closser, K. D.; Prendergast, D.; Leone, S. R. Femtosecond X-Ray Spectroscopy of an Electrocyclic Ring-Opening Reaction. *Science* **2017**, *356*, 54−59.

(4) Bhattacherjee, A.; Schnorr, K.; Oesterling, S.; Yang, Z.; Xue, T.; de Vivie-Riedle, R.; Leone, S. R. Photoinduced Heterocyclic Ring Opening of Furfural: Distinct Open-Chain Product Identification by Ultrafast X-Ray Transient Absorption Spectroscopy. *J. Am. Chem. Soc.* **2018**, *140*, 12538−12544.

(5) Yang, Z.; Schnorr, K.; Bhattacherjee, A.; Lefebvre, P.-L.; Epshtein, M.; Xue, T.; Stanton, J. F.; Leone, S. R. Electron-Withdrawing Effects in the Photodissociation of CH_2ICl To Form CH_2Cl Radical, Simultaneously Viewed Through the Carbon K and Chlorine $L_{2,3}$ X-Ray Edges. *J. Am. Chem. Soc.* **2018**, *140*, 13360−13366.

(6) Scutelnic, V.; Tsuru, S.; Pápai, M.; Yang, Z.; Epshtein, M.; Xue, T.; Haugen, E.; Kobayashi, Y.; Krylov, A. I.; Møller, K. B.; Coriani, S.; Leone, S. R. X-Ray Transient Absorption Reveals the ^1A_u ($n\pi^*$) State of Pyrazine in Electronic Relaxation. *Nat. Commun.* **2021**, *12*, No. 5003.

(7) Ross, A. D.; Hait, D.; Scutelnic, V.; Haugen, E. A.; Ridente, E.; Balkew, M. B.; Neumark, D. M.; Head-Gordon, M.; Leone, S. R. Jahn-Teller Distortion and Dissociation of CCl_4^+ by Transient X-Ray Spectroscopy Simultaneously at the Carbon K- and Chlorine L-Edge. *Chem. Sci.* **2022**, *13*, 9310−9320.

(8) Haugen, E. A.; Hait, D.; Scutelnic, V.; Xue, T.; Head-Gordon, M.; Leone, S. R. Influence of Electron Withdrawing Groups on Ultrafast Intersystem Crossing by Transient X-Ray Absorption Spectroscopy at the Carbon K-Edge. *J. Phys. Chem. A* **2023**, *127*, 634−644.

(9) Epshtein, M.; Scutelnic, V.; Yang, Z.; Xue, T.; Vidal, M. L.; Krylov, A. I.; Coriani, S.; Leone, S. R. Table-Top X-Ray Spectroscopy of Benzene Radical Cation. *J. Phys. Chem. A* **2020**, *124*, 9524−9531.
(10) Vidal, M. L.; Epshtein, M.; Scutelnic, V.; Yang, Z.; Xue, T.; Leone, S. R.; Krylov, A. I.; Coriani, S. Interplay of Open-Shell Spin-Coupling and Jahn−Teller Distortion in Benzene Radical Cation Probed by X-Ray Spectroscopy. *J. Phys. Chem. A* **2020**, *124*, 9532−9541.
(11) Palmer, M. H.; Ridley, T.; Hoffmann, S. V.; Jones, N. C.; Coreno, M.; de Simone, M.; Grazioli, C.; Zhang, T.; Biczysko, M.; Baiardi, A.; Peterson, K. Interpretation of the Photoelectron, Ultraviolet, and Vacuum Ultraviolet Photoabsorption Spectra of Bromobenzene by Ab Initio Configuration Interaction and DFT Computations. *J. Chem. Phys.* **2015**, *143*, No. 164303.
(12) Schneider, M.; Soshnikov, D. Y.; Holland, D. M. P.; Powis, I.; Antonsson, E.; Patanen, M.; Nicolas, C.; Miron, C.; Wormit, M.; Dreuw, A.; Trofimov, A. B. A Fresh Look at the Photoelectron Spectrum of Bromobenzene: A Third-Order Non-Dyson Electron Propagator Study. *J. Chem. Phys.* **2015**, *143*, No. 144103.
(13) Baltzer, P.; Karlsson, L.; Wannberg, B.; Öhrwall, G.; Holland, D. M. P.; MacDonald, M. A.; Hayes, M. A. Von Niessen, W. An Experimental and Theoretical Study of the Valence Shell Photoelectron Spectrum of the Benzene Molecule. *Chem. Phys.* **1997**, *224*, 95−119.
(14) Powis, I.; Holland, D. M. P.; Antonsson, E.; Patanen, M.; Nicolas, C.; Miron, C.; Schneider, M.; Soshnikov, D. Y.; Dreuw, A.; Trofimov, A. B. The Influence of the Bromine Atom Cooper Minimum on the Photoelectron Angular Distributions and Branching Ratios of the Four Outermost Bands of Bromobenzene. *J. Chem. Phys.* **2015**, *143*, No. 144304.
(15) Hitchcock, A. P.; Pocock, M.; Brion, C. E.; Banna, M. S.; Frost, D. C.; McDowell, C. A.; Wallbank, B. Inner Shell Excitation and Ionization of the Monohalobenzenes. *J. Electron Spectrosc. Relat. Phenom.* **1978**, *13*, 345−360.
(16) Hitchcock, A. P.; Fischer, P.; Gedanken, A.; Robin, M. B. Antibonding. σ^* Valence MOs in the Inner-Shell and Outer-Shell Spectra of the Fluorobenzenes. *J. Phys. Chem. A* **1987**, *91*, 531−540.
(17) Schwarz, W. H. E.; Chang, T. C.; Seeger, U.; Hwang, K. H. Core Excitations of Symmetrical Aromatic Molecules. Specific Correlations in the Valence Shell and Localization in the Core Shells. *Chem. Phys.* **1987**, *117*, 73−89.
(18) Plashkevych, O.; Yang, L.; Vahtras, O.; Ågren, H.; Petterson, L. G. Substituted Benzenes as Building Blocks in Near-Edge X-Ray Absorption Spectra. *Chem. Phys.* **1997**, *222*, 125−137.
(19) Roemelt, M.; Maganas, D.; DeBeer, S.; Neese, F. A Combined DFT and Restricted Open-Shell Configuration Interaction Method Including Spin-Orbit Coupling: Application to Transition Metal L-Edge X-Ray Absorption Spectroscopy. *J. Chem. Phys.* **2013**, *138*, No. 204101.
(20) Becke, A. D. Density-functional Thermochemistry. III. The Role of Exact Exchange. *J. Chem. Phys.* **1993**, *98*, 5648−5652.
(21) Schäfer, A.; Horn, H.; Ahlrichs, R. Fully Optimized Contracted Gaussian Basis Sets for Atoms Li to Kr. *J. Chem. Phys.* **1992**, *97*, 2571−2577.
(22) Coutinho, L. H.; de Ribeiro, F. A.; Tenorio, B. N. C.; Coriani, S.; dos Santos, A. C. F.; Nicolas, C.; Milosavljevic, A. R.; Bozek, J. D.; Wolff, W. NEXAFS and MS-AES Spectroscopy of the C 1s and Cl 2p Excitation and Ionization of Chlorobenzene: Production of Dicationic Species. *Phys. Chem. Chem. Phys.* **2021**, *23*, 27484−27497.
(23) Benitez, A.; Moore, J. H.; Tossell, J. A. The Correlation between Electron Transmission and Inner Shell Electron Excitation Spectra. *J. Chem. Phys.* **1988**, *88*, 6691−6698.
(24) Püttner, R.; Kolczewski, C.; Martins, M.; Schlachter, A. S.; Snell, G.; Sant'Anna, M.; Viefhaus, J.; Hermann, K.; Kaindl, G. The C1s NEXAFS Spectrum of Benzene below Threshold: Rydberg or Valence Character of the Unoccupied σ-Type Orbitals. *Chem. Phys. Lett.* **2004**, *393*, 361−366.
(25) Kolczewski, C.; Püttner, R.; Martins, M.; Schlachter, A. S.; Snell, G.; Sant'Anna, M. M.; Hermann, K.; Kaindl, G. Spectroscopic Analysis of Small Organic Molecules: A Comprehensive Near-Edge X-Ray-Absorption Fine-Structure Study of C_6-Ring-Containing Molecules. *J. Chem. Phys.* **2006**, *124*, No. 034302.
(26) Holland, D. M. P.; Edvardsson, D.; Karlsson, L.; Maripuu, R.; Siegbahn, K.; Potts, A. W.; von Niessen, W. An Experimental and Theoretical Study of the Valence Shell Photoelectron Spectrum of Bromobenzene. *Chem. Phys.* **2000**, *252*, 257−278.
(27) Krylov, A. I. Triradicals. *J. Phys. Chem. A* **2005**, *109*, 10638−10645.
(28) Hait, D.; Haugen, E. A.; Yang, Z.; Oosterbaan, K. J.; Leone, S. R.; Head-Gordon, M. Accurate Prediction of Core-Level Spectra of Radicals at Density Functional Theory Cost via Square Gradient Minimization and Recoupling of Mixed Configurations. *J. Chem. Phys.* **2020**, *153*, No. 134108.
(29) Lindblad, R.; Kjellsson, L.; Couto, R. C.; Timm, M.; Bülow, C.; Zamudio-Bayer, V.; Lundberg, M.; von Issendorff, B.; Lau, J. T.; Sorensen, S. L.; et al. X-Ray Absorption Spectrum of the N_2^+ Molecular Ion. *Phys. Rev. Lett.* **2020**, *124*, No. 203001.
(30) Couto, R. C.; Kjellsson, L.; Ågren, H.; Carravetta, V.; Sorensen, S. L.; Kubin, M.; Bülow, C.; Timm, M.; Zamudio-Bayer, V.; von Issendorff, B.; et al. The Carbon and Oxygen K-Edge NEXAFS Spectra of CO^+. *Phys. Chem. Chem. Phys.* **2020**, *22*, 16215−16223.
(31) Kwon, C. H.; Kim, H. L.; Kim, M. S. Vibrational Spectra of Halobenzene Cations in the Ground and $\tilde{B}^2B_2$ Electronic States Obtained by One-Photon Mass-Analyzed Threshold Ionization Spectrometry. *J. Chem. Phys.* **2002**, *116*, 10361−10371.
(32) Fally, S.; Carleer, M.; Vandaele, A. C. UV Fourier Transform Absorption Cross Sections of Benzene, Toluene, Meta-, Ortho-, and Para-Xylene. *J. Quant. Spectrosc. Radiat. Transfer* **2009**, *110*, 766−782.
(33) Etzkorn, T.; Klotz, B.; Sørensen, S.; Patroescu, I. V.; Barnes, I.; Becker, K. H.; Platt, U. Gas-Phase Absorption Cross Sections of 24 Monocyclic Aromatic Hydrocarbons in the UV and IR Spectral Ranges. *Atmos. Environ.* **1999**, *33*, 525−540.
(34) Kadi, M.; Davidsson, J.; Tarnovsky, A. N.; Rasmusson, M.; Åkesson, E. Photodissociation of Aryl Halides in the Gas Phase Studied with Femtosecond Pump-Probe Spectroscopy. *Chem. Phys. Lett.* **2001**, *350*, 93−98.

https://doi.org/10.1021/jacs.2c12334
J. Am. Chem. Soc. 2023, 145, 3554−3560